Constant Frequency Torque and Flux controllers for Direct Torque Control of Induction Machines

N. R. N. Idris, A. H. M. Yatim, N. D. Muhamad and T. C. Ling
Electrical Energy Conversion Department,
Universiti Teknologi Malaysia,
81310 UTM, Skudai, MALAYSIA

Abstracts – This paper proposed a simple solution to the variable switching frequency and high torque ripples problems encountered in hysteresis-based DTC drives. The method replaces the hysteresis-based controllers with fixed switching controllers, which operate based on the comparison between the error signals and the triangular waveforms. Implementation of these controllers using digital circuits is highly suitable since they only require comparisons of waveforms rather than calculations of duty cycles or voltage vectors. Modeling and simulation of the DTC drives using these simple controllers are presented and the results show that they are capable of reducing the torque ripples significantly.

I. Introduction

More than a decade ago, direct torque control (DTC) was introduced to give a fast and good dynamic torque response and can be considered as an alternative to the field oriented control (FOC) technique [1,2,3]. Since it was introduced, most of the researches carried out on DTC drives were mainly to improve their performance. Among the major problems that are usually associated with DTC drives are the variable switching frequency of the power devices used for the voltage source inverter and high torque ripples [4,5].

In hysteresis-based controller with fixed hysteresis band, the switching frequency depends on the rate of change of the torque and flux (or the slope of torque and flux). This is because different slopes will result in a different time taken for both torque and flux to reach their upper and lower bands. The slopes depend on several factors, which are the speed, stator and rotor fluxes, loads and dc link voltage [6,7]. It is possible to calculate the extreme cases corresponding to the maximum switching frequency, however if most of the time the drive operates other than this extreme cases, the capability of the switching devices will be under-utilized. Various solutions have been proposed to overcome this problem. In [8], a variable hysteresis bands has been proposed so that the bands can be adjusted to maintain a constant switching frequency. In [9,10,11], constant switching frequency is achieved by using space vector modulation technique whereas in [12,13,14] controlled duty cycle was introduced. All of these schemes have managed to produce a constant switching frequency but at the same time have significantly increased the complexity of the DTC drive systems.

DTC drives based on hysteresis controllers also suffer from high torque ripples. Even with small hysteresis bands, the torque ripples are still high due to the delays in the feedback due to microprocessor implementations [4]. A simple solution to this is achieved by increasing the sampling period of the microprocessor as shown in [15]. A more popular solution is to use non hysteresis-based controllers such as the use of predictive control scheme [12,13,14] space vector modulation and dead-beat control [9,10,11]. In all these methods, the processor used in the implementation will be burdened with the calculations of the appropriate duty cycles or voltage vectors in order to minimize the torque ripples. It is also interesting to note that the various methods of torque ripples reduction works simply because the torque switching frequency is increased. In other words, if the switching frequency of the torque controller can be increased, then to some extent it can also be said that the torque ripples can also be reduced. In fact, it is shown in [16] that by introducing dithering signals superimposed to the torque and flux errors, which effectively increase the torque and flux switching frequencies, the torque and flux ripples were significantly reduced.

This paper proposes a simple method of obtaining a constant switching frequency and reducing torque ripples in DTC drives. It is accomplished by introducing a new torque and flux controllers to replace the hysteresis-based controllers. This means that the simple structure of DTC as initially proposed is retained. The new controllers are based on the comparisons between compensated error signals with high frequency triangular waveforms. The switching frequencies of the torque and flux controllers are fixed to the respective triangular frequency and therefore independent from the operating conditions. Implementation of these controllers using digital hardware is highly suitable since it only requires comparison of waveforms rather than calculations of duty cycles or voltage vectors. The rest of the paper is organized as follows. Section II outlines the equations for the torque and flux slopes. Section III introduces the proposed controllers while section IV discusses on the selection of the controllers' parameters. Section V presents the simulation results of the proposed controllers and finally, conclusions are given in section VI.

II. Torque and Flux Slopes

In order to analyze the DTC drive in terms of its switching frequency and torque ripples, the following induction machine equations written in general reference frame are used:

$$\bar{v}_s^g = R_s \bar{i}_s^g + \frac{d\bar{\psi}_s^g}{dt} + j\omega_g \bar{\psi}_s^g \qquad (1)$$

0-7803-7754-0/03/$17.00 ©2003 IEEE

$$0 = R_r \bar{i}_r^g + \frac{d\bar{\psi}_r^g}{dt} + j(\omega_g - \omega_r)\bar{\psi}_r^g \quad (2)$$

In the above equations, $\bar{\psi}_s^g$ and $\bar{\psi}_r^g$ are the stator and rotor flux linkages respectively and are given by:

$$\bar{\psi}_s^g = L_s \bar{i}_s^g + L_m \bar{i}_r^g \quad (3)$$

$$\bar{\psi}_r^g = L_r \bar{i}_r^g + L_m \bar{i}_s^g \quad (4)$$

The super-script 'g' in the above equations denotes that the quantity is referred to the general reference frame. The torque and mechanical dynamics of the machine are modeled by the following:

$$T_e = \frac{3}{2}\frac{p}{2}\bar{\psi}_s^g \times \bar{i}_s^g \quad (5)$$

$$J\frac{d\omega_m}{dt} = J\frac{2}{p}\frac{d\omega_r}{dt} = T_e - T_{load} \quad (6)$$

Using equations (1) – (6), in stationary reference frame, it can be shown that the positive and negative torque slopes are given by [6]:

$$\frac{dT_e^+}{dt} = -T_e\left(\frac{1}{\sigma\tau_s} + \frac{1}{\sigma\tau_r}\right) + \frac{3}{2}\frac{p}{2}\frac{L_m}{\sigma L_s L_r}\left(\bar{v}_s - j\omega_r\bar{\psi}_s\right) \bullet j\psi_r \quad (7)$$

$$\frac{dT_e^-}{dt} = -T_e\left(\frac{1}{\sigma\tau_s} + \frac{1}{\sigma\tau_r}\right) - \frac{3}{2}\frac{p}{2}\frac{L_m}{\sigma L_s L_r} j\omega_r\bar{\psi}_s \bullet j\psi_r \quad (8)$$

Equations (7) and (8) indicate that torque slope depends on the rotor speed, rotor and stator fluxes and voltage vectors. With variable torque slope, the time taken for the torque to reach its upper and lower hysteresis bands will also varies and hence resulted in switching frequency, which depend on operating conditions.

If the stator resistance drop is neglected, using (3), the slope of the flux in stationary reference frame can be approximated by (9) which simply indicate that it is totally depends on the selected voltage vectors.

$$\text{slope} \equiv \frac{d\Psi}{dt} = \bar{v}_s \quad (9)$$

The slope at any instant equals the tangential component of the selected voltage vectors to the circular stator flux locus – which means that it is highly dependent on the stator flux position. If the stator flux lie in sector k and assuming that voltage vectors k+1 and k+2 are selected to increase and decrease the flux respectively, then the positive and negative slope over a sector at the any instant an active voltages is applied are given by (10). This is illustrated in Fig. 1.

$$\left.\begin{aligned} \text{slope}^+ &\equiv \frac{2}{3}V_{dc}\sin\theta \\ \text{slope}^- &\equiv -\frac{2}{3}V_{dc}\sin(\theta + \frac{2}{3}\pi) \end{aligned}\right\} \quad \text{for } 0 < \theta < \pi/3 \quad (10)$$

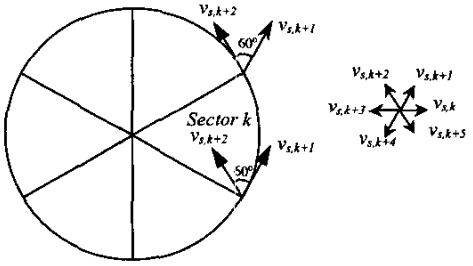

Fig. 1 Selection of voltage vectors in sector k

where θ in (10) is the angle between the circular stator flux locus and the voltage vectors. The flux slope equations indicate that the slope is independent of the speed, flux magnitude and loads but only depends on the selected voltage vectors. Thus for hysteresis-based flux controller, the number of switching of a flux controller over one cycle depends on the width of the hysteresis flux and also on the synchronous speed.

III. Proposed Controllers

The proposed controller is based on the observations described in the preceding section. That is, avoiding the use of hysteresis-based controller and performing the switching at high frequency in order to establish a fixed switching frequency and reduced the torque ripples, respectively. Both the flux and torque controllers are switched at regular intervals and are independent of operating conditions in particular to the rotor speed.

A. Torque controller

The proposed torque controller consists of two triangular waveform generators, two comparators and a PI controller as shown in Fig. 2. The two triangular waveforms (C_{upper} and C_{lower}) are 180° out of phase with each other. The absolute values of the DC offsets for the triangular waveforms are set to half of their peak-peak values. In principle, the output of the proposed torque controller is similar to that of the three level hysteresis comparator [1], which can be either of three states: –1 , 0 or 1.

The value of the instantaneous output of the torque controller designated by $q_t(t)$ is given by (11). For a triangular period of T_{tri}, its averaged value which will be designated by $d_t(t)$ is given by (12).

$$q_t(t) = \begin{cases} 1 & \text{for } T_c \geq C_{upper} \\ 0 & \text{for } C_{lower} < T_c < C_{upper} \\ -1 & \text{for } T_c \leq C_{lower} \end{cases} \quad (11)$$

$$d_t(t) = \frac{1}{T_{tri}}\int_t^{t+T_{tri}} q(t)\,dt \quad (12)$$

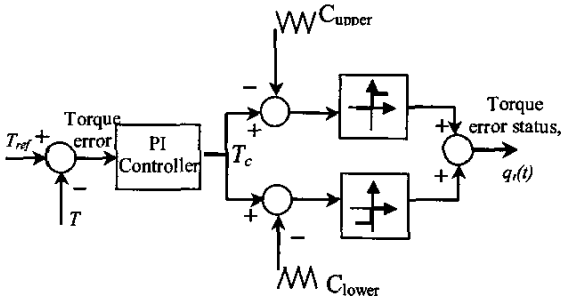

Fig. 2 Proposed torque controller

B. *Flux controller*

The proposed flux controller is shown in Fig 3, which in principle works similar to that of the torque controller. As in the hysteresis-based controller, there are only two levels of output generated from the controller, i.e. 1 to increase the flux and 0 to reduce the flux. This implies that only single triangular waveform is required. For a given synchronous frequency, the switching frequency of the flux controller only depends on the triangular waveform frequency. The output of the controller, termed as flux error status, is given by:

$$q_f(t) = \begin{cases} 1 & \text{for } F_c \geq C_{upper} \\ 0 & \text{for } F_c < C_{upper} \end{cases} \quad (13)$$

For a triangular period of T_{tri}, its average value is given by:

$$d_f(t) = \frac{1}{T_{tri}} \int_{t}^{t+T_{tri}} q(t)\, dt \quad (14)$$

IV. Controllers Disign

The controllers used for the torque and flux regulation are designed based on linear control system theory. For this, the torque and flux loops have to be modeled, averaged and linearized.

A. *Torque controller*

It can be shown that the relation between the torque error, $T_c(s)$, and d(s) is equal to the reciprocal of the peak-peak of the triangular waveform.

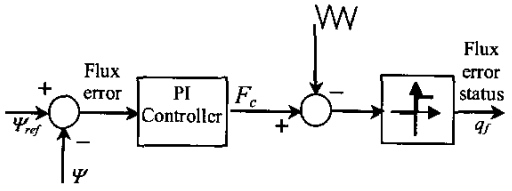

Fig. 3 Proposed flux controller

The task is therefore to obtain the transfer function between d(s) and T(s). For this, equations (7) and (8), has to be averaged and linearized. The torque slopes of (7) and (8) written in d-q components are given by:

$$\frac{dT_e^+}{dt} = -\frac{T_e}{\sigma\tau_{sr}} + \frac{3}{2}\frac{p}{2}\frac{L_m}{\sigma L_s L_r}\left[-v_{ds}\psi_{qr} + v_{qs}\psi_{dr} - \omega_r \cdot \left(\psi_{ds}\psi_{dr} + \psi_{qs}\psi_{qr}\right)\right] \quad (15)$$

$$\frac{dT_e^-}{dt} = -\frac{T_e}{\sigma\tau_{sr}} - \frac{3}{2}\frac{p}{2}\frac{L_m}{\sigma L_s L_r}\omega_r\left[\psi_{ds}\psi_{dr} + \psi_{qs}\psi_{qr}\right] \quad (16)$$

In stator flux reference frame such that $\Psi_{qs} = 0$ as shown in Fig. 4, these equations can be written as (17) and (18). This particular reference frame is indicated by the superscript 'ψs'.

$$\frac{dT_e^+}{dt} = -\frac{T_e}{\sigma\tau_{sr}} + \frac{3p}{4}\frac{L_m}{\sigma L_s L_r}\left[v_s^{\psi s}\psi_s - (\omega_r - \omega_{\psi s}) \cdot (\psi_s \psi_r^{\psi s})\right] \quad (17)$$

$$\frac{dT_e^-}{dt} = -\frac{T_e}{\sigma\tau_{sr}} - \frac{3p}{4}\frac{L_m}{\sigma L_s L_r}\left[(\omega_r - \omega_{\psi S}) \cdot (\psi_s \psi_r^{\psi S})\right] \quad (18)$$

The term $\omega_{\psi s}$ in the above equations is the instantaneous stator flux angular frequency and is given by:

$$\omega_{\psi s} = \frac{\Delta\theta}{\Delta t} \quad (19)$$

In (19), $\Delta\theta$ is a small change in stator flux angle when an active voltage vector is applied for Δt second. This can be easily calculated since we know that the number of active voltage vectors selected over one synchronous cycle is given by $2\pi f_{tri} / \omega_e$, where ω_e is the synchronous frequency. Therefore

$$\frac{\Delta\theta}{\Delta t} = \frac{\left(\frac{2\pi\omega_e}{2\pi f_{tri}}\right)}{\frac{d}{f_{tri}}} = \frac{\omega_e}{d} \quad (20)$$

This instantaneous stator flux angular can be written in terms of slip and rotor frequency as:

$$\omega_{\psi s} = \frac{\omega_{slip} + \omega_r}{d} \quad (21)$$

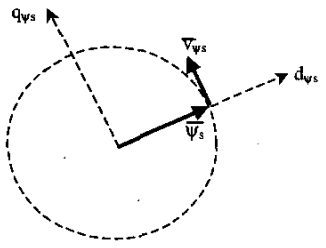

Fig. 4 Instantaneous stator flux reference frame

For simplicity, in this particular reference frame, two assumptions are made: the d components of the voltage vectors are zero and the load angle (angle between rotor and stator flux) is negligibly small. The latter implies that the *d* component of the rotor flux equals its modulus, i.e. $\Psi_{dr} = |\Psi_r|$. Substituting (21) and applying these assumptions, the torque equations (20) and (21) can be written as:

$$\frac{dT_e^+}{dt} = -A_t T_e + B_t v_s^{\psi s} + K_t\left(\frac{\omega_e}{d} - \omega_r\right) \tag{22}$$

$$\frac{dT_e^-}{dt} = -A_t T_e - K_t \omega_r \tag{23}$$

where $A_t = \frac{1}{\sigma\tau_{sr}}$ $\quad B_t = \frac{3p}{4}\frac{L_m}{\sigma L_s L_r}\psi_s$

$$K_t = \frac{3p}{4}\frac{L_m}{\sigma L_s L_r}(\psi_s \psi_r^{\psi_s})$$

Equations (22) and (23) are averaged and simplified to give:

$$\frac{dT_e}{dt} = -A_t T_e + B_t v_s^{\psi s} d + K_t(\omega_{slip}) \tag{24}$$

Equation (24) can now be transformed to frequency domain and linearized by introducing small perturbation in T_e, d and ω_{slip}. The torque, T_e therefore can be written as:

$$\tilde{T}_e(s) = \frac{B_t v_s^{\psi s}\tilde{d}(s) + K_t\tilde{\omega}_{slip}(s)}{s + A_t} \tag{25}$$

The term contributed by the slip frequency is relatively small and hence for simplicity will be neglected. The complete torque loop is shown in Fig 5. Ideally, the torque loop bandwidth should be as large as possible to obtain fast torque response. However this bandwidth and hence the selection of controller's parameters (proportional gain K_{tp}, and integral gain K_{ti}) is limited by several constraints, as will be discussed in the next section.

It should also be noted that this simplified model only serves as a guide to the controller's parameters selection. A fine tune of the controller can be achieved by means of simulation.

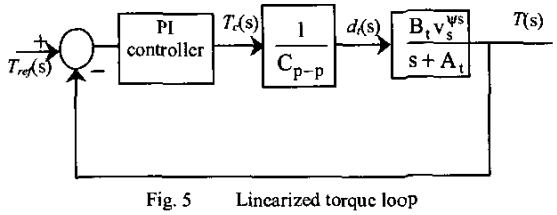

Fig. 5 Linearized torque loop

B. *Flux controller*

According to (10), the flux slope varies with flux position and repeats for every sector. For simplicity it will be assumed that the slope is constant during which the flux error status is 1 or 0. Then, it is possible to obtain the average positive and negative slopes by averaging them over a sector. This is easily done since we know the number of positive or negative slopes within a sector is given by $N_f = (2\pi f_{tri})/6\omega_e$. The average positive and negative slope can be calculated as:

$$\frac{d\Psi^+}{dt} = \frac{1}{N_f}\sum_{n=0}^{N_f}\frac{2}{3}V_{dc}\sin\left(\frac{\frac{\pi}{3}}{N_f}\right)n = A_\psi \tag{26}$$

$$\frac{d\Psi^-}{dt} = -\frac{1}{N_f}\sum_{n=0}^{N_f}\frac{2}{3}V_{dc}\sin\left(\left(\frac{\frac{\pi}{3}}{N_f}\right)n + \frac{2}{3}\pi\right) = B_\psi \tag{27}$$

Which gives an average slope of:

$$\frac{d\Psi}{dt} = (A_\psi - B_\psi)d + B_\psi \tag{28}$$

Introducing small perturbation in ψ and d, the transfer function between ψ and d can be obtained as:

$$\frac{\tilde{\Psi}}{\tilde{d}} = \frac{(A_\psi - B_\psi)}{s} \tag{29}$$

Finally, the linearized flux loop is shown as in Fig 6.

V. Selection of Controllers' Parameters and Some Simulation Results

Simulations for both hysteresis-based and proposed controllers are carried out using Matlab/Simulink simulation package. The parameters of a 1.5 kW induction machine used in the simulation are given in Table 1. To simulate delays caused by microprocessor implementation, the voltage and currents used for flux and torque estimations are sampled using a *sample and hold* block from the Simulink library If the output signals of the controllers are assumed to be constant within a triangular period, then the sampling of the calculated torque and flux errors for comparison with the triangular is synchronized to the peak of the respective triangular waveforms.

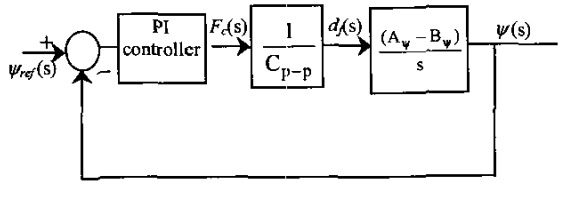

Fig. 6 Linearized flux loop

TABLE 1
INDUCTION MACHINE USED FOR SIMULATION

Stator resistanace	5.5 Ω
Rotor resistance	4.51 Ω
Stator self inductance	306.5 mH
Rotor self inductance	306.5 mH
Mutual inductance	291.9mH
Rated speed	1410 rpm
Pole	4
V_{dc}	654 V

The triangular frequencies of the torque and flux controllers are set to 20 kHz and 10 kHz respectively, each with a peak-peak of 100 units. Based on the motor's parameters of Table 1, the numerical values of the parameters for the torque and flux loops are calculated and tabulated in Table 2.

TABLE 2
PARAMETERS FOR THE FLUX AND TORQUE LOOPS

A_t	351
B_t	111
K_t	130
A_ψ	212
B_ψ	-203

For comparison purposes, hysteresis-based DTC drive is also simulated with a sampling time set to 20μs.

The triangular slope limits the proportional gain, K_{tp}. For 20 kHz, the slope of the triangular is 4 x 10^6 Nm/s. Therefore K_{tp} is calculated such that the torque slopes of (22) and (23) times K_{tp} does not exceed the triangular slope, as given by (30) and (31).

$$\langle \text{absolute slope of the carrier} \rangle \geq \left\{ -A_t T_e + B_t V_s^{\psi s} + K_t \left(\frac{\omega_s}{d} - \omega_r \right) \right\} K_{tp}^{+} \quad (30)$$

$$\langle \text{absolute slope of the carrier} \rangle \geq \left| -A_t T_e - K_t \omega_r \right| K_{tp}^{-} \quad (31)$$

Substituting values with extreme cases into equations (30) and (31) gives K^{+}_{tp} = 57 K^{-}_{tp} = 175. The smaller value of K_{tp}, i.e. 57, is selected since this will ensure that the slope of the signal coming out of the PI controller will not exceed the slope of the triangular waveform. The integral gain K_{ti} is selected such the zero of the PI controller cancels the pole of the open loop gain.

The integral part of the controller for the flux loop is not required since the open-loop gain consists of only an integral and a gain. If the bandwidth is too low, flux ripple at 6 x the synchronous frequency (f_e) due to the variation of flux slope with flux position will appear in the flux response. The bandwidth of the flux loop and hence the triangular frequency, therefore must be set such that it is at least 7 to 8 times larger than 6 x f_e. If f_e is taken as the nominal frequency, than the bandwidth is 8 x 6 x (50) = 2400 Hz. Which means that the triangular frequency must be set at least 4800 Hz. In order to minimize the 6 x fe ripples in the flux waveform, the triangular frequency is set to 10 kHz. This permits a flux loop bandwidth of approximately 5 kHz. There are two limitations, which must be considered when selecting the proportional gain of the controller. The first limitation is the slope of the output of the proportional controller, which must be ensured not to exceed the triangular slope. At 10 kHz, the absolute slope of the triangular with peak-peak value of 100 is 2 x 10^6. According to (10), the maximum absolute values of the positive and negative slopes are equal and occur at $\pi/3$ and 0, respectively – with V_{dc} = 654V, it is equal to 378. Thus, the maximum K_{fp} under this constraint is 5.3 x 10^3. The second limitation is on the closed-loop bandwidth of the flux loop, which must be ensured not to exceed half of the triangular frequency. With the help of a bode plot, it is found that the maximum value of K_{fp} for maximum bandwidth of 5 kHz is 5 x 10^3. To ensure that the slope of the error signal coming from the proportional controller does not exceed the slope of the triangular waveform, the value of 5 x 10^3 for K_{fp} is used.

Fig. 7 shows the torque response of the proposed and hysteresis-based controllers with a ±10 Nm square wave torque reference. The simulation results demonstrate the effectiveness of the proposed torque controller in reducing the torque ripples. Further reducing the hysteresis (for the hysteresis-based controller) will not reduce the torque ripple since the overshoot in the torque causes reverse voltage vectors selected, instead of zero vectors. The results also indicate that the dynamic torque response of the proposed controller is as good as the hysteresis-based controller. Fig. 9 (a) gives a closer view of the torque as well as the triangular waveforms, which are compared with the output of the PI controller. Fig. 8 (b) shows the hystersis-based controller under the same condition. Fig.9 (a) and (b) show the simulation results of the flux locus for the proposed controller and the hysteresis-based controller ($\Delta\psi$=0.03 Wb), respectively.

Experimental set-up to verify the effectiveness of the proposed controllers is under development. The proposed hardware implementation consists of hybrid analog and digital circuits utilizing Altera FPGA.

VI. CONCLUSIONS

The paper has presented the new torque and flux controllers with constant switching frequencies. Modeling of the torque and flux loops, which involved averaging and linearizing torque and flux equations, has been presented. From the simulation results, it is shown that the proposed controllers have managed to reduce the torque ripples significantly. Since the controllers operate based on comparison of waveforms, implementation using hybrid analog and digital circuits is highly suitable. Works on the implementation of the proposed controllers are under development.

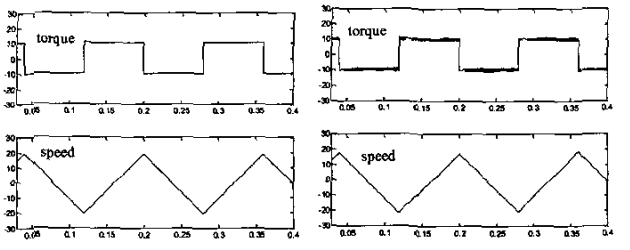

(a) (b)

Fig. 7 Torque and speed response. (a) proposed controller, (b) hysteresis-based controller (ΔT = 1 Nm)

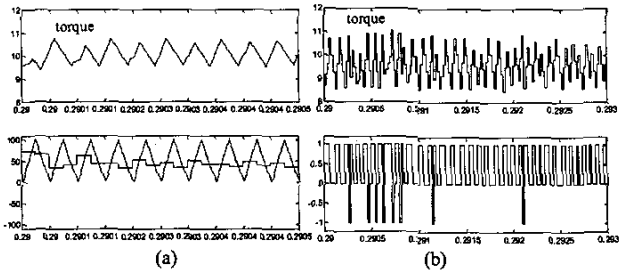

(a) (b)

Fig. 8 Waveforms of proposed and hysteresis-based controllers. (a) proposed controller – upper trace: torque, lower trace: upper triangular waveform and and T_c (b) hysteresis-based controller with ΔT = 1 Nm – upper trace: torque, lower trace: torque error status

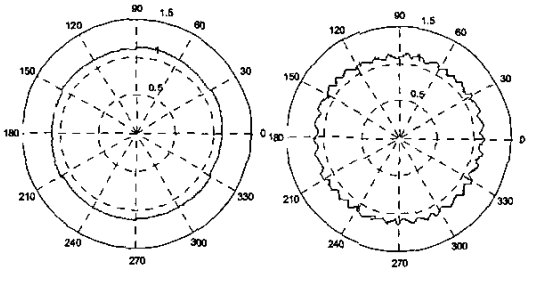

(a) (b)

Fig. 9 Steady state flux locus. (a) proposed flux, (b) hysteresis-based ($\Delta\Psi$ = 0.03 Wb).

References

[1] I. Takahashi and T. Noguchi, "A new quick-response and high-efficiency control strategy of an induction motor", IEEE Trans. Ind. Appl., Vol. IA-22, No 5, pp. 820-827, 1986

[2] P. Tiitinen and M. Surandra, "The next generation motor control method, DTC direct torque control", Proceedings of the 1996 International Conference on Power Electronics, Drives and Energy Systems for Industrial Growth, Vol. 1 , pp 37 -43, 1996.

[3] D. Casadei, F. Profumo and A. Tani, "FOC and DTC: two viable schemes for induction motors torque control", IEEE Transactions on Power Electronics, Volume: 17 Issue: 5 , pp. 779 –787, Sept. 2002

[4] N.N.R.Idris and A.H.M Yatim, "Reduced torque ripple and constant torque switching frequency direct torque control of induction machines", 15th IEEE-Applied Power Electronics Conference and Exhibition 2000 (APEC 2000), New Orleans, USA, Feb. 2000.

[5] D. Casadei, G. Grandi, G. Serra and A. Tani; "Effects of flux and torque hysteresis band amplitude in direct torque control of induction machines", 20th International Conference on Industrial Electronics, Control and Instrumentation IECON '94, Vol. 1 , pp 299 -304, 1994.

[6] D. Casadei;G. Serra.and A. Tani "Analytical investigation of torque and flux ripple in DTC schemes for induction motors", 23rd International Conference on Industrial Electronics, Control and Instrumentation, IECON 97., Vol. 2 , pp. 552 –556, 1997

[7] J–W. Kang and S. K. Sul, "Analysis and prediction of inverter switching frequency in direct torque control of induction machine based on hysteresis bands and machine parameters", IEEE Transactions on Industrial Electronics, Vol. 48, No. 3 , pp. 545 –553, Jun 2001

[8] J–W. Kang, D–W Chung and S. K. Sul, "Direct torque control of induction machine with variable amplitude control of flux and torque hysteresis bands", International Conference on Electric Machines and Drives IEMD '99 , pp. 640 –642, 1999.

[9] T. G. Habetler, F. Profumo, M. Pastorelli and L. M. Tolbert, "Direct torque control of induction machines using space vector modulation", Conference Record of the Industry Applications Society Annual Meeting, Vol. 1, pp. 428 - 436, 1991

[10] D. Casadei,G. Serra and A. Tani, "Improvement of direct torque control performance by using a discrete SVM technique", 29th Annual IEEE Power Electronics Specialists Conference PESC 98, Vol. 2 , pp. 997-1003, 1998.

[11] Lixin Tan and M. F. Rahman, "A new direct torque control strategy for flux and torque ripple reduction for induction motors drive by using space vector modulation", 32nd Annual Power Electronics Specialists Conference PESC. 2001, Vol. 3 , pp. 1440 –1445, 2001

[12] Y. Li., J. Shao and B. Si, "Direct torque control of induction motors for low speed drives considering discrete effect of control and dead-time timing of inverters", IEEE-IAS Annual Meeting, pp. 781-788, 1997.

[13] S. Mir, and M. E. Elbuluk, "Precision torque control in inverter-fed induction machines using fuzzy logic", IEEE-IAS Annual Meeting, pp. 396-401, 1995.

[14] I. G. Bird, and H. Zelaya De La Parra, "Fuzzy logic torque ripple reduction for DTC based AC drives", Electronic Letters, Vol. 33, No.17, pp. 1501-1502, 1997

[15] A. Purcell and P. Acarnley, " Device switching scheme for direct torque control", Electronics Letters , Vol. 34, Issue 4 , pp. 412 –414, 1998.

[16] T. Noguchi, M. Yamamoto, S. Kondo and I. Takahashi, "High frequency switching operation of PWM inverter for direct torque control of induction motor", Conference Record of the Industry Applications Annual Meeting IAS '97, Vol. 1 , pp. 775 780, 1997.